Design and Locomotion of a Semi-Passive Mobile Platform

Amir Shapiro[1] and Shraga Shoval[2]

[1] Department of Mechanical Engineering, Ben Gurion University of the Negev, Beer Sheva 84105, Israel. `ashapiro@bgu.ac.il`

[2] Department of Industrial Engineering & Management, College of Judea and Samaria, Ariel 44837, Israel. `shraga@yosh.ac.il`

Summary. This paper presents a novel design and a motion planner for a semi-passive mobile robot. The robot consists of an upper circular body and three identical semi-passive driving mechanisms. Each mechanism consists of a passive wheel that can freely roll, a rotation actuator along the normal axes and a linear actuator for motion along the radial direction of the upper body center. The robot is equipped with an inclinometer to measure the surface slope. Each wheel is also equipped with a rotational encoder to measure roll. Using an odometric model, data from these encoders determines vehicle position. Kinematic analysis provides tools for designing a motion path that steers the robot to the desired location, and determines the singular configurations. Due to the passive roll, there is no longitudinal slippage, and lateral slippage is determined from the kinematic and odometric models. This enables accurate and reliable localization even with slippage. A gait pattern planer for downhill, as well as horizontal and uphill surfaces is presented. A prototype robot has been built and field tested. Experimental results verify the suggested models.

Key words: passive motion planning, skid steering, slippage.

1 Introduction

Wheel slippage is one of the dominant features that affect the efficiency, reliability, feasibility and stability of mobile robot motion. Uncontrolled slippage causes undesired motions that result in erroneous position and orientation. The most common method for autonomous relative position estimate - odometry, is subject to unbounded errors due to slippage [2], and requires an additional positioning system (e.g. Map-Matching, GPS, Beacon-Based Triangulation). This problem becomes critical when no absolute positioning system is available (e.g. space, underground or indoor missions). Furthermore, additional tasks such as trajectory planning and obstacle avoidance cannot be reliably performed in the presence of uncontrolled slippage. Many researchers deal with robot-surface interaction, particularly on slippery terrains. Bidaud et. al. [1] deal with wheel-soil interaction models. Iagnemma et. al. [7] describe terrain estimation and sensing methodology using visual, tactile and

vibrational feedback. Ferretti et. al. [5] exploits high resolution encoders to compensate for non linear friction terms. Physics based motion control that involves a model of traction mechanics with the consideration of force distribution among the wheels is discussed in [3]. In this approach the wheel-soil contact angle and the distribution of the load on each wheel are considered, and a control system maximizes traction between the vehicle and the terrain. Yoshida and Hammano [11] investigate the tire-soil traction mechanics as well as the body-suspension-wheel dynamics of a mobile robot.

Conventional locomotion uses legs or powered wheels to generate motion. In contrast, our robot relies on relative motion of the joints to generate motion of the central body similar to the motion of a downhill skier on an icy surface, or locomotion on rollerblades. A novel robot design that has the ability to switch between skating and walking modes is the Roller-Walker [4]. This quadruped robot has the ability to switch between walking and skating modes. Passive wheels at the end of each leg fold flat to allow the robot to walk. In the skating mode, the wheels are rotated into place to allow the robot to carry out skating motion. Another example is the ROLLERBLADER [6]. This robot is different from the Roller Walker in its ability to raise the rollerblades off the ground. This allows the use of gaits that mimic those used by human rollerbladers. Shimizu [10] developed both a skiing robot and a snowboarding robot that can model how humans perform turns on skis or snowboard.

Semi-passive driving mechanism has several advantages over regular powered mechanisms. First, no longitudinal slippage occurs, given minimal friction between the wheels and the surface. The minimal friction is required for overcoming the rotational friction between the wheels and their housing, which is significantly reduced even by conventional bearings. The elimination of longitudinal slippage is essential for accurate and reliable odometry, particularly for outdoor missions. Using semi passive driving mechanism, combined with intelligent motion planner can significantly reduce the power consumption of the vehicle. Utilizing the powered mechanism only when required (e.g. traveling uphill or on horizontal surface), while changing to passive motion when possible (downhill travel or using the vehicle inertia) can save significant energy consumption, and therefore increase the autonomy of the system. Finally, while replacing the passive wheels with ice skating blades it can move on slippery surfaces such as ice utilizing the unique characteristic of small friction forces on the longitudinal direction and large friction forces on the lateral direction.

The paper is organized as follows: In Section 2 we describe the robot design. Section 3 provides kinematic analysis and geometrical insights of singular configurations under no lateral slippage conditions. Section 4 suggests an odometric model for localization and lateral slippage detection. Section 5 describes motion patterns for downhill, uphill and horizontal locomotion. Section 6 presents experimental results that verify the motion planner and the odometric model. Section 7 provides the conclusions.

2 Robot Description

The robot consists of an upper circular body and three identical semi-passive driving mechanisms shown in Fig. 1(a). Each driving mechanism consists of a passive wheel that rolls freely along its longitudinal direction. The mechanism has two actuators: a rotational and a linear actuators shown in Fig. 1(b). Both actuators use Pittman DC servo motors. The linear actuators use a lead screw mechanism with two parallel slide guides and linear bearings. The rotational actuator uses timing belt mechanism to reduce the total robot height and lower the center of gravity. The robot is equipped with studded-like tires to increase traction and reduce slippage. The wheels can be easily replaces by ice skating blades or skis for motion on icy or snowy surfaces. The robot is equipped with an inclinometer to measure the surface slope.

The robot is equipped with six degrees of freedom, allowing for changes in the internal configuration which are required for various motion patterns (as described in the following sections). The rotation along the normal to the central body determines the longitudinal rolling direction of the wheel. Since wheels are passive, we assume no longitudinal slippage (lateral slippage is permitted)[3]. Each of the passive wheels is equipped with a rotational encoder to measure rolling. Data from these encoders is used by the odometric model for relative position and orientation estimation of the robot. Furthermore, based on the kinematic and odometric models (discussed in Sections 3 and 4), the amount of lateral slippage on each wheel can be determined.

3 Kinematic Analysis

The robot's c-space (configuration space) contains nine parameters, $\mathbf{q} = (x_b, y_b, \theta_b, d_1, d_2, d_3, \theta_1, \theta_2, \theta_3) \in I\!R^9$, out of which only six are actuated. Hence the robot's central base is un-actuated. The goal is to design a motion path for the actuated joints such that it steers the entire robot to a desired location. To begin, we compute each wheel's center point location and velocity using rigid body transformation and its time derivative:

$$\mathbf{p}_i = \mathbf{d}_b + R_b d_i \mathbf{r}_i \ \text{ and } \ \dot{\mathbf{p}}_i = \dot{\mathbf{d}}_b + R_b \dot{d}_i \mathbf{r}_i - \dot{\theta}_b J R_b d_i \mathbf{r}_i \quad \text{ for } i = 1, 2, 3 \quad (1)$$

where $J = \begin{bmatrix} 0 & 1 \\ -1 & 0 \end{bmatrix}$ and R_b is the rotation matrix of the central base angle θ_b. *Assuming no lateral slippage*, the wheel's center point velocity has no component along the lateral direction. Therefore:

$$\mathbf{c}_i^T \dot{\mathbf{p}}_i = \mathbf{0} \quad \text{ for } i = 1, 2, 3 \quad (2)$$

where $\mathbf{c}_i = R_b R_i (1, 0)^T$ is the lateral direction of the ith wheel, and R_i is the wheel's rotation matrix of angle θ_i. Let us make the following definitions:

---

[3] This assumption is valid only for wheels with small inertia and for relatively small accelerations.
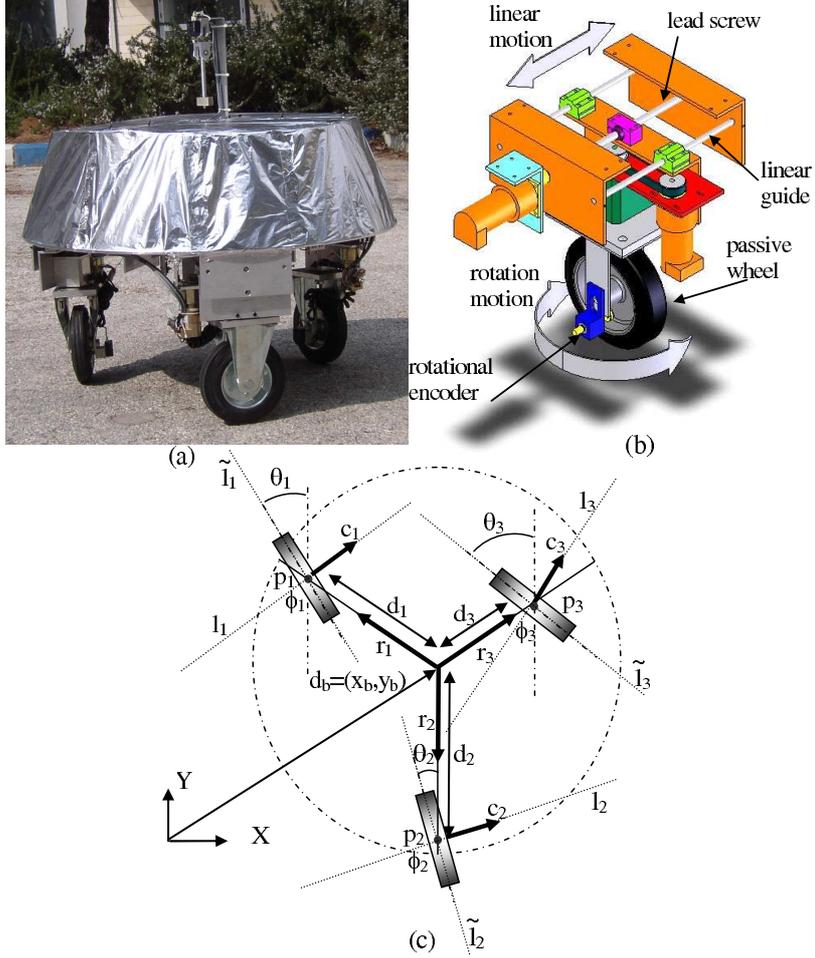
Fig. 1. (a) Prototype of the three wheeled robot, (b) design model of the wheel mechanism, and (c) the robot's parameters.

$$V(\mathbf{q}) = -diag(\mathbf{c}_1^T R_b \mathbf{r}_1, \mathbf{c}_2^T R_b \mathbf{r}_2, \mathbf{c}_3^T R_b \mathbf{r}_3) \in I\!\!R^{3\times3} \qquad (3)$$

and

$$K(\mathbf{q}) = \begin{bmatrix} \mathbf{c}_1^T & -d_1 \mathbf{c}_1^T J R_b \mathbf{r}_1 \\ \mathbf{c}_2^T & -d_2 \mathbf{c}_2^T J R_b \mathbf{r}_2 \\ \mathbf{c}_3^T & -d_3 \mathbf{c}_3^T J R_b \mathbf{r}_3 \end{bmatrix} \in I\!\!R^{3\times3}.$$

The no-slippage constraint (2) can now be written in matrix form as follows:

$$\begin{pmatrix} \dot{\mathbf{d}}_b \\ \dot{\theta}_b \end{pmatrix} = G(\mathbf{q}) \begin{pmatrix} \dot{d}_1 \\ \dot{d}_2 \\ \dot{d}_3 \end{pmatrix} \quad \text{where} \quad G(\mathbf{q}) = K^{-1}(\mathbf{q}) V(\mathbf{q}) \in I\!\!R^{3\times3}. \qquad (4)$$

This constraint depends on velocities as well as on the configuration. Therefore, (4) introduces three non-holonomic constraints, and the robot is said to be a *non-holonomic, under-actuated system*. Let $\mathbf{u} = (\mathbf{u}_d, \mathbf{u}_\theta)^T \in I\!R^6$ be vector of control inputs, where $\mathbf{u}_d = (\dot{\mathbf{d}}_1, \dot{\mathbf{d}}_2, \dot{\mathbf{d}}_3)^T$ and $\mathbf{u}_\theta = (\dot{\boldsymbol{\theta}}_1, \dot{\boldsymbol{\theta}}_2, \dot{\boldsymbol{\theta}}_3)^T$. Then the robot's kinematic system is:

$$\dot{\mathbf{q}} = \begin{pmatrix} G(\mathbf{q})\mathbf{u}_d \\ \mathbf{u} \end{pmatrix}. \tag{5}$$

The central base velocity is uniquely determined by the actuators' velocities only if $G(\mathbf{q})$ has full rank. Moreover, existence and uniqueness of solution to the robot's kinematic system is assured only if $rank(K(\mathbf{q})) = 3$. Matrix $K(\mathbf{q})$ is of full rank if, and only if, the three lines l_1, l_2, and l_3 do not intersect in a single point and are not mutually parallel. Theses lines are given by $\mathbf{l}_i = \mathbf{p}_i + t_i\mathbf{c}_i$ for $i = 1, 2, 3$, and t_i is a length parameter along the ith line (Fig. 1(c)). If the robot is not in a singular configuration, the central base velocity is fully controllable using the linear actuators velocities. Later on we use this fact to conduct uphill motion. However, singular configuration can be used for free slide in downhill motion.

4 Odometric Model and Slippage Detection

In this section we describe the odometric model of the robot and a method for slippage detection. As previously discussed, each wheel is equipped with a rotational encoder to measure the passive roll - ϕ_i, (Fig. 1(c)). Given the central body velocity, the wheels' center point velocity is computed in (1). Taking the derivative of ϕ_i and multiplying by the wheel radius - W_r, gives the ith wheel center point longitudinal velocity. Equating the latter term with the ith wheel center point velocity projected on the longitudinal direction, denoted $\tilde{\mathbf{c}}_i = -J\mathbf{c}_i$, results in:

$$\tilde{\mathbf{c}}_i^T \dot{\mathbf{p}}_i = \dot{\phi}_i W_r \quad \text{for } i = 1, 2, 3 \tag{6}$$

Based on (6) it is possible to evaluate the central base velocities while measuring the passive wheels' rotation velocities and the actuators' positions and velocities. Let us define the 3×3 matrix $\tilde{K}(\mathbf{q})$ as follows:

$$\tilde{K}(\mathbf{q}) = \begin{bmatrix} \tilde{\mathbf{c}}_1^T & -d_1\tilde{\mathbf{c}}_1^T JR_b\mathbf{r}_1 \\ \tilde{\mathbf{c}}_2^T & -d_2\tilde{\mathbf{c}}_2^T JR_b\mathbf{r}_2 \\ \tilde{\mathbf{c}}_3^T & -d_3\tilde{\mathbf{c}}_3^T JR_b\mathbf{r}_3 \end{bmatrix} \in I\!R^{3 \times 3}, \tag{7}$$

then central base velocity is determined by:

$$\begin{pmatrix} \dot{x}_b \\ \dot{y}_b \\ \dot{\theta}_b \end{pmatrix} = \tilde{K}^{-1}(\mathbf{q}) \begin{pmatrix} \dot{\phi}_1 W_r - \dot{d}_1\tilde{\mathbf{c}}_1^T R_b\hat{\mathbf{r}}_1 \\ \dot{\phi}_2 W_r - \dot{d}_2\tilde{\mathbf{c}}_2^T R_b\hat{\mathbf{r}}_2 \\ \dot{\phi}_3 W_r - \dot{d}_3\tilde{\mathbf{c}}_3^T R_b\hat{\mathbf{r}}_3 \end{pmatrix}.$$

Numerical integration of the central base velocity along the motion path determines the robot's central base position. Note that as long as $\tilde{K}(\mathbf{q})$ is

not singular it is possible to calculate the base position *even under lateral slippage*. Matrix $\tilde{K}(\mathbf{q})$ is of full rank if, and only if, the three lines $\tilde{l}_1, \tilde{l}_2$, and $\tilde{l}_3$ do not intersect in a single point and are not mutually parallel, where $\tilde{\mathbf{l}}_i = \mathbf{p}_i + \tilde{t}_i\tilde{\mathbf{c}}_i$ for $i = 1, 2, 3$, and $\tilde{t}_i$ is a length parameter along the $\tilde{l}_i$ line (Fig. 1(c)).

Slippage detection method: After evaluating the central body velocities, it is possible to compute each wheels' center point velocity according to (1). This velocity vector, $\dot{\mathbf{p}}_i$, can be divided into two components: the longitudinal component, $\tilde{\mathbf{c}}_i^T\dot{\mathbf{p}}_i$, and the radial component,

$$\dot{s}_i = \mathbf{c}_i^T\dot{\mathbf{p}}_i \quad \text{for} \quad i = 1, 2, 3.$$

Note that $\dot{s}_i$ is the lateral velocity of the wheel center point. If the three lines $\tilde{\mathbf{l}}_1, \tilde{\mathbf{l}}_2$ and $\tilde{\mathbf{l}}_3$ (Fig. 1(c)) do not intersect in a single point and are not mutually parallel, then *we can explicitly compute the amount of lateral slippage of each wheel.*

5 Motion Patterns

In this section we describe the motion patterns of the robot. Since motion is based on a semi-passive mechanism, there are two major patterns: Uphill and horizontal locomotion, and downhill motion.

### 5.1 Uphill and Horizontal Locomotion

In horizontal or uphill locomotion, gravitational force cannot be used to conduct motion. Rather, the robot actuators produce the required central body velocity. The motion planning problem is as follows: For a given path, $\boldsymbol{\alpha}(t)$ of the robot's central body, what should be the actuators' velocities. The Lafferriere and Sussmann method [9] is an example of such a motion planning method for under-actuated non-holonomic systems. The Lafferriere and Sussmann method requires the system to be nilpotent (i.e. high order of Lie products vanish). However, our system contains trigonometric function whose derivatives never vanish and therefore is not nilpotent. Eq.(4) shows that, in order to provide the robot's central body with any desired velocity, the linear joints should supply the joint's velocities

$$\mathbf{u}_d = V^{-1}(\mathbf{q})K(\mathbf{q})\begin{pmatrix}\dot{\mathbf{d}}_b \\ \dot{\theta}_b\end{pmatrix}_{desired} \quad \text{where} \quad \begin{pmatrix}\dot{\mathbf{d}}_b \\ \dot{\theta}_b\end{pmatrix}_{desired} = \dot{\boldsymbol{\alpha}}(t). \quad (8)$$

Applying the velocities described in (8) to the linear actuators provides the central body with the desired velocity and it precisely follows the $\boldsymbol{\alpha}(t)$ path. This motion is limited by the linear actuators' stroke. When one of the linear actuators reaches its limit, all actuators stop. Next, the linear actuators return to their initial configuration without causing the robot's central body to move. From (3) we notice that if the matrix $V(\mathbf{q})$ is the 3×3 zero matrix, motion of

the linear actuators will not affect motion of the robot's central body. $V(\mathbf{q})$ is a diagonal matrix with the terms $\mathbf{c}_i^T R_b \mathbf{r}_i$ on the diagonal. The $\mathbf{c}_i^T R_b \mathbf{r}_i$ terms vanish if each $\mathbf{c}_i$ is perpendicular to $R_b \mathbf{r}_i$. This happens only when the wheels are in the radial directions.

Figure 2 illustrates the principle of our motion patterns for linear motion and for circular motion around the robot's center. Motion consists of four steps, in which some or all wheels change their angular and/or linear configuration resulting in the desired path for the robot's central body. Other trajectories can be generated using similar patterns.
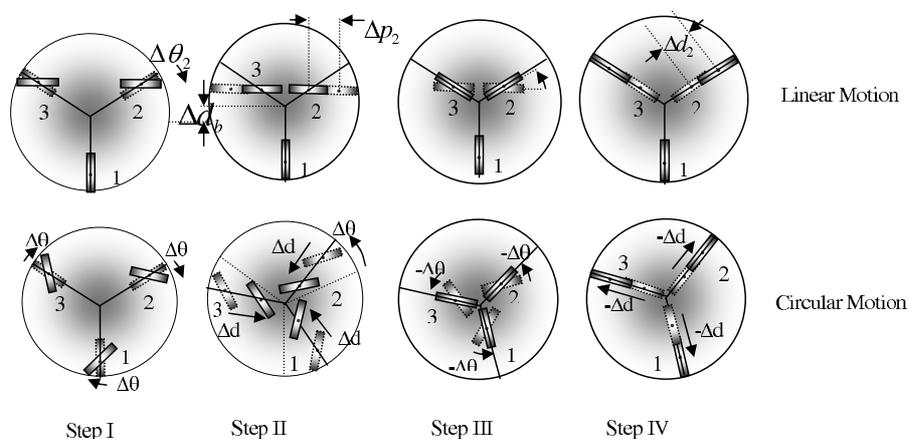
Fig. 2. Horizontal and uphill motion patterns

Linear motion pattern consists on four phase motion: First the front two wheels (wheels 2 and 3) rotate $\Delta\theta_2$ and $\Delta\theta_3$ to the required configuration (Step I). Next, the linear actuators of wheels 2 and 3 move to provide the desired velocity to the central body (step II). The actuators move Δd_2 and Δd_3, resulting in a longitudinal motion of wheels 2 and 3 of Δp_2 and Δp_3, and a central body linear motion of Δd_b. It should be noted that $\Delta p_2 = \Delta p_3 = \Delta d_2 \cos\Delta\theta_3$, and $\Delta d_b = \Delta d_2 \sin\Delta\theta_3$. Once the linear actuators reach their maximum stroke, the wheels rotate such that their longitudinal axes coincide with the radial direction to the base center (in our case $-\Delta\theta_2$ and $-\Delta\theta_3$). Finally, the linear actuators return to their initial configuration.

Circular motion pattern: In the first step all wheels simultaneously rotate $\Delta\theta$ at the same direction. Next, all linear actuators move simultaneously the same distance Δd. This linear motion generates tangential forces that rotate the robot's body $\Delta\theta_b$ around its center. Once the linear actuators reach their limit, the wheels rotate such that their longitudinal axes coincide with the radial direction to the base center and the linear actuators return to their

initial configuration. The rotation around the robot center $\Delta\theta_b$ is given by

$$\Delta\theta_b = \frac{\Delta d}{d}\tan(\Delta\theta)$$

where d is distance between the robot center and the wheels. According to this equation, larger rotation angle of the wheels $\Delta\theta$ in step I increases the rotation of the robot's body in step II. However, $\Delta\theta = 90°$ is a singular configuration in which the body can rotate freely with around its center. It also should be noted that as the wheels approach the robot's center, the rotation rate increases for the same $\Delta\theta$. However, the friction forces required for this rotation increase, and eventually break the static friction constraint, resulting in a lateral slippage of the wheels.

Other trajectories can be generated using similar patterns. For example, a rotation around one of the robot's wheels is shown in Figure 3 (in this figure around wheel 3). In step I wheel 2 rotate $60°$ and wheel 3 rotate 90^circ to the configuration shown. Next, the linear actuator of wheel 1 generates the rotation of the body by moving d_1. In step III the wheels rotate back to the radial configuration and in step IV the linear actuator of wheel 1 returns to the initial configuration.
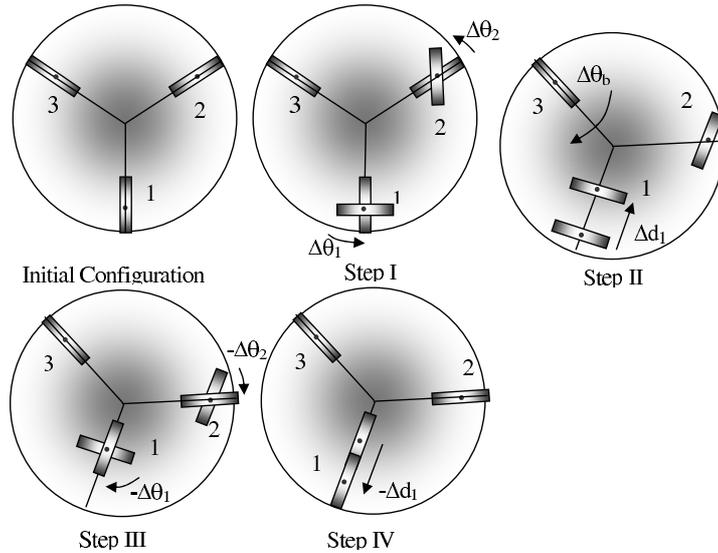
Fig. 3. Motion pattern for rotation about wheel 3.

5.2 Downhill Locomotion

In downhill motion the gravitational force is used for dragging the robot downwards. For circular motion the lines $\mathbf{l}_i$'s intersect in a single point and the

matrix $K(\mathbf{q})$ is singular. In this case the robot is constrained to move along an arc shaped path. The center of the arc is in the intersection point of the $\mathbf{l}_1,\mathbf{l}_2$ and $\mathbf{l}_3$ lines. Since the robot is an Euler-Lagrange system and since there is friction in the wheels' bearings, the system is passive and governed by gravitational potential energy. According to Koditschek [8] the configuration in which the system's potential energy is minimal is an asymptotical stable equilibrium point of the system. According to this observation, we find the radius and center of curvatures at each point of the desired motion path. Then we continuously set the $\mathbf{l}_i$'s intersection point at the center of curvature of the desired path by changing the robot's configuration. This way, the robot passively glides along the desired path. In the "snow-plough" motion two wheels are rotated in a "snow-plough" configuration, while the third wheel is used for steering. In this mode, speed is controlled according to the slide angle of the wheels relative to the motion direction. Figure 4 shows these two patterns for downhill motion.
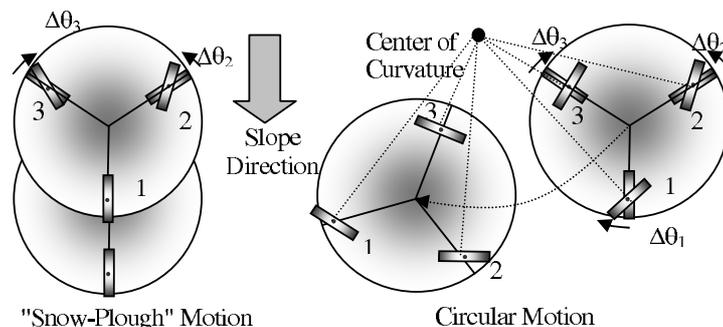

Fig. 4. Downhill motion patterns

6 Experimental Results

In this section we describe the experiments conducted with our autonomous robot, shown in Figure 1(a).

In the first experiment we examine the linear motion pattern on a horizontal surface. Figure 5 shows the robot configuration (rotation angle and linear actuator of all wheels) during motion. Wheels 2 and 3 perform the required rotation and translation as shown in figure 2, while wheel 1 remains passive. The second part of figure 5 shows the actual wheels locations during motion as determined by our odometric model. Although the nominal path of the robot center is linear, actual path is not linear and bends to the right. This is expected as the experiment is conducted on a non-homogenous surface, and lateral slippage occurs, especially during stage II. This is also the reason for the oscillated motion of wheel 1, which nominally remains passive during that motion. However, the slippage is clearly detected by the odometric model.
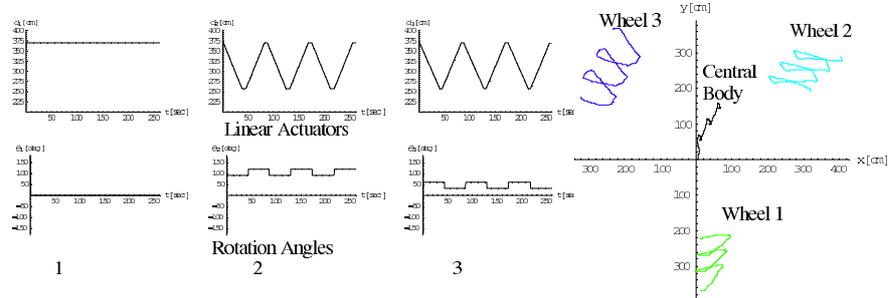
Fig. 5. Actual paths determined by the odometric model in horizontal linear motion

Figure 6 shows the robot configuration (rotation angle and linear actuator of all wheels) during circular motion around the center of the robot. Instead of returning to initial configuration (Step III in Figure 2) all wheels are rotated $-2\Delta\theta$ before the linear actuators return. This way rotation of the central body continues during Step IV, resulting in a double rotation angle for a full motion period.
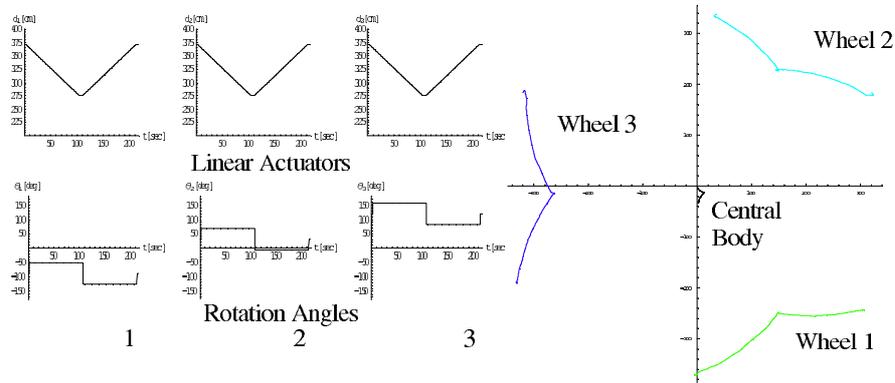

Fig. 6. Actual paths determined by the odometric model in horizontal circular motion

Figure 7 shows a downhill motion using the "snow-plough" method. In this motion all linear actuators remains stationary, and wheels 2 and 3 are rotated until motion starts. Returning to the initial radial configuration stops the motion. The odometric model shows identical, parallel and near-linear motion of all wheels and robot's body. The non-linearity of the path occurs at the beginning and end of motion due to rotation of the wheels.

Finally we show an experiment for downhill rotation. In the experiment shown in figure 8, the robot rotates around wheel 3 according to the pattern
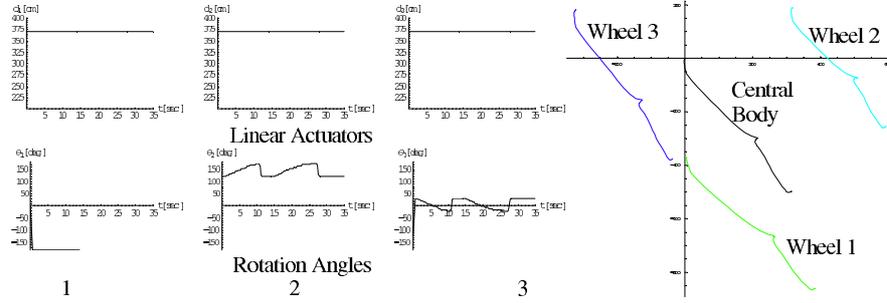
Fig. 7. Actual paths determined by the odometric model in linear downhill motion

shown in figure 4. In this pattern wheels 1 and 2 rotate $\Delta\theta_i$ such that $\mathbf{l}_1$ and $\mathbf{l}_2$ (lines through wheels 1 and 2 in the lateral direction) intersect at the contact point of wheel 3. The robot rotates about wheel 3 and stops when in reaches a minimal potential energy position.
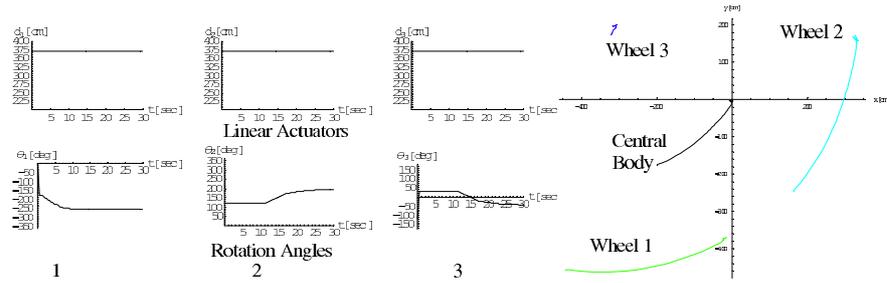

Fig. 8. Actual paths determined by the odometric model in linear downhill motion

7 Conclusions

In this paper we present a mobile robot, designed for motion on slippery surfaces. Motion is performed by changes in the internal configuration of the robot, using passive rolling studded-like wheels. Kinematic model determines the required joints' velocities that steer the robot to a target position. Odometric model accurately determines the robot's position even in the presence of slippage. A method for evaluating the lateral slippage based on the odometric and kinematic models is presented. Gait patterns for motion up and down hills, as well as on horizontal surface are presented. Experimental results verify our models and slippage estimate, and show the reliability and accuracy of motion on slippery surfaces. Field experiments for the suggested

gait patterns on various slopes and terrains have been carried out using our prototype model. In future work we intend to develop a dynamic model and investigate the effect of various terrain types on the suggested gait patterns.

References

1. P. Bidaud, R. Chatila, G. Andrade-Barroso, and F. Ben Amar. Modeling robot-soil interaction for planetary rover motion control. In *IEEE/RSJ Int. Conf. on Intelligent Robots and Systems*, pages 576–581, Victoria B.C., Canada, October 1998.
2. J. Borenstein and L. Feng. Gyrodometry: A new method for combining data from gyros and odometry in mobile robots. In *IEEE Int. Conf. on Robotics and Automation*, pages 423–428, Minneapolis, Minnessota, April 1996.
3. S. Dubowsky and K. Iagnemma. Mobile robot rough-terrain control (rtc) for planetary exploration. In *Proceedings of ASME DETC/CIE: 26th Biennial Mechanisms and Robotics Conference*, Baltimore, Maryland, September 2000.
4. G. Endo and S. Hirose. Study on roller-walker (multi-mode steering control and self-contained locomotion). In *IEEE Int. Conf. on Robotics and Automation*, pages 2808–2814, San Francisco, CA, April 2000.
5. G. Ferretti, G. Magnani, G. Martucci, P. Rocco, and V. Stampacchia. Friction model validation in sliding and presliding regimes with high resolution encoders. In *Experimental Robotics VIII B. Siciliano and P. Dario Eds.*, pages 328–337. STAR Springer, Heidelberg, 2002.
6. C. Frederik, W. Heger, and V. Kumar. Design and gait control of a rollerblading robot. In *IEEE Int. Conf. on Robotics and Automation*, pages 3944–3949, New Orleans, LA, April 2004.
7. K. Iagnemma and S. Dubowsky. Vehicle wheel-ground contact angle estimation: with application to mobile robot traction control. In *7th Int. Symposium on Advances in Robot Kinematics*, Piran-Portoroz, Slovenia, June 2000.
8. D. E. Koditschek. The application of total energy as a lyapunov function for mechanical control systems. *In J. Marsden, Krishnaprasad, and J. Simo, editors, Control Theory and Multibody Systems, AMS Series in Contemporary Mathematics*, 97:131–158, 1989.
9. G. Lafferriere and H. J. Sussman. A differential geometry approach to motion planning. In *Nonholonomic Motion Planning Z. Li and J. F. Canny Eds.*, pages 235–270. Kluwer, 1993.
10. S. Shimizu, K. Hasegawa, and T. Nagasawa. Alpine ski robot. *Journal of Robotics Society of Japan (JRSJ) special issue on Amusement Robot*, 8(3):126, June 1990.
11. K. Yoshida and H. Hamano. Motion dynamics of a rover with slip-based traction model. In *IEEE Int. Conf. on Robotics and Automation*, pages 3155–3160, Washington D.C., May 2002.